




Optical properties of yellow-emitting $\text{Sr}_3\text{LaNb}_3\text{O}_{12}:\text{Dy}^{3+}$ phosphors with an abnormal thermal quenching for white light-emitting diode applications

Yuchen Zhang¹, Zhikai Liang^{2,5}, Weixian Wang¹, Yifang Lin¹, Rong Tang³, Jingfei Wang¹, Daomiao He¹, Jinhui Liu¹, Zhong Zhang³, Lingzhi Zhao⁴, Bin Deng^{2,5,*}, Dan Zhang^{1,*} , and Ruijin Yu³

¹ College of Science, Northwest A&F University, Yangling 712100, Shaanxi, People's Republic of China

² School of Chemistry and Environmental Science, Xiangnan University, Chenzhou 423043, Hunan, People's Republic of China

³ College of Chemistry & Pharmacy, Northwest A&F University, Yangling 712100, Shaanxi, People's Republic of China

⁴ SCNU Qingyuan Institute of Science and Technology Innovation Co., Ltd, Qingyuan 511517, Guangdong, People's Republic of China

⁵ Hunan Provincial Key Laboratory of Xiangnan Rare-Precious Metals Compounds Research and Application, Xiangnan University, Chenzhou 423043, Hunan, People's Republic of China

Received: 11 August 2022

Accepted: 20 October 2022

Published online:

13 November 2022

© The Author(s), under exclusive licence to Springer Science+Business Media, LLC, part of Springer Nature 2022

ABSTRACT

In this study, a series of $\text{Sr}_3\text{LaNb}_3\text{O}_{12}$ phosphors doped with Dy^{3+} ions was prepared by a high-temperature solid-state reaction. The crystal structure, phase purity, particle morphology, photoluminescence (PL) properties, and thermal stability of the phosphors were described. And the $\text{Sr}_3\text{LaNb}_3\text{O}_{12}$ crystal symmetry is hexagonal. Under the optimal excitation wavelength of 352 nm, the three prominent emission peaks of the $\text{Sr}_3\text{LaNb}_3\text{O}_{12}:\text{Dy}^{3+}$ focused on 483 nm ($^4\text{F}_{9/2}-^6\text{H}_{15/2}$), 575 nm ($^4\text{F}_{9/2}-^6\text{H}_{13/2}$), and 668 nm ($^4\text{F}_{9/2}-^6\text{H}_{11/2}$). The optimal Dy^{3+} -doped concentration in the $\text{Sr}_3\text{LaNb}_3\text{O}_{12}$ phosphor was 0.05 mol. The phosphor had an abnormal thermal quenching phenomenon and activation energy ($E_a = 0.29$ eV). The prepared white light-emitting diode (w-LED) had a low correlation color temperature of 4162 K, chromaticity coordinates (0.365, 0.368), and the color rendering index 91. The feasibility of the $\text{Sr}_3\text{LaNb}_3\text{O}_{12}:\text{Dy}^{3+}$ luminescent material for w-LED was verified by its performance.

Yuchen Zhang and Zhikai Liang contributed equally to this work.

Address correspondence to E-mail: dengbinxnu@163.com; danzhang@nwafu.edu.cn

<https://doi.org/10.1007/s10854-022-09374-4>

1 Introduction

White light-emitting diodes (W-LEDs) have the advantages of low energy consumption, environmental protection, and higher efficiency, which remedies some disadvantages of incandescent and traditional fluorescent lamps [1–8]. Nowadays, commercial w-LEDs are based on blue light-emitting diode (LED) chips using the YAG:Ce³⁺. The blue chips may take a toll on health [9, 10]. For example, it leads to the inhibition of melatonin secretion, myopia, and yellow spots [11, 12]. The phosphor conversion to n-UV chips stimulating w-LEDs can solve these problems. Therefore, it is of great significance to develop a new yellow phosphor for w-LEDs based on n-UV chips.

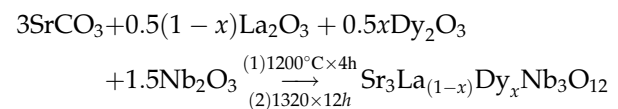
In recent years, Dy³⁺ ions doped phosphors have been studied for w-LED in many rare-earth ions. And Dy³⁺ ions doped phosphors have good optical properties in many reports [13–15]. The rare-earth Dy³⁺ ions are highly efficient activators and usually have a blue peak, prominent yellow emission peak, and low-intensity red emission peak, corresponding to ⁴F_{9/2}-⁶H_{1/2} (J = 15, 13, 11) transitions [16–18]. White light is obtained by taking the host materials and doped Dy³⁺ ions in combination. Emission peaks of rare-earth Dy³⁺ ions doped materials can show white light and the CIE coordinates can be reflected in the white light area. Therefore, many Dy³⁺-doped materials are ideally combined with an n-UV chip and successfully applied in the w-LED [19–21].

An excellent host material favors the luminescence properties of doped ions. The hexagonal perovskite Sr₃LaNb₃O₁₂ is a good microwave dielectric material with low loss, whose space group is *R*₃*m*. At present, many hexagonal perovskite phosphors are applied in w-LEDs. Peng et al. compounded Sr₃La(VO₄)₃:Sm³⁺ phosphors which have good thermal stability [22]. Priyanka et al. researched the luminescence properties of Dy³⁺-activated BaYAlZn₃O₇ phosphors, a fine cold-white-emitting material [23]. Zhang et al. studied luminescence properties and the thermal stability of Sr₂CaLa(VO₄)₃:Sm³⁺ phosphors with higher activation energy [24]. These show that the phosphors with hexagonal perovskite structures have good optical properties. However, the luminescence properties of Sr₃LaNb₃O₁₂:Dy³⁺ phosphors haven't been studied.

Here, novel Dy³⁺-doped Sr₃LaNb₃O₁₂ phosphors were compounded by a solid-state reaction. The structural and optical properties of phosphors were researched, including phase purity, crystal structure, particle morphology, element composition, CIE chromaticity coordinates, photoluminescence properties, and the abnormal thermal stability [25–27]. Finally, w-LEDs were prepared using multicolor phosphors based on an n-UV chip.

2 Experimental section

Dy³⁺-doped Sr₃La_{1-x}Dy_xNb₃O₁₂ (*x* = 0.01, 0.02, 0.05, 0.10, 0.15, 0.20, 0.25, and 0.30 mol) phosphors were prepared by the traditional high-temperature solid-state technique. High purity raw materials were SrCO₃ (99%), La₂O₃ (99.99%), Dy₂O₃ (99.99%), and Nb₂O₅ (99.9%). These raw materials were weighed by following the equilibrium equation and ground for around 16 min in the agate mortar. Then the samples were put in the small crucibles. The samples firstly were heated at 1200 °C for four hours in the muffle furnace. When the preparation firing reaction was completed, they were cooled to room temperature. Afterward, the prepared samples were continued to be heated at 1320 °C for twelve hours. After a series of reactions were completed, the samples were fetched and completely smashed. Then color and hardness of products were recorded and used for the next luminescence characterization. The related experimental equation is given as follows:



The phase purity analysis of Sr₃LaNb₃O₁₂:*x*Dy³⁺ (*x* = 0.01–0.30 mol) phosphors were revealed on the X-ray diffractor (XRD, Bruker D2 PHASER) with Cu Kα source (*λ* = 0.154184 nm) by scanning from 10° to 70° range. The crystal structure was refined the Maud software. The sample particle size was obtained passing by a laser particle size analyzer (Malvern MS2000). The appearance and composition of the phosphor element were determined with scanning electron microscopy (Nova Nano SEM-450) equipped with energy-dispersive X-ray spectrum (EDS). The photoluminescence (PL) spectra and temperature-dependent spectra were measured via Edinburgh

FLS 980 spectrometer, which used a 450 W Xenon lamp as the excitation source.

The prepared yellowing $\text{Sr}_3\text{LaNb}_3\text{O}_{12}:0.05\text{Dy}^{3+}$ phosphor was mixed with a bit of commercial red phosphor ((Sr, Ca)AlSiN₃:Eu²⁺) and blue phosphor (BaMgAl₁₀O₁₇:Eu²⁺ (BAM)) to obtain the required mixture, whose ratio is 98%, 0.5%, and 1.5%, respectively. The mixture was added with a moderate amount of shadowless adhesive and combined with a 388 nm n-UV InGaN chip. The obtained product was cured under a UV lamp for 5 min, and finally, the w-LED can be fabricated. Then CIE chromaticity coordinates, electroluminescence (EL) spectrum, R_a , and correlation color temperature (CCT) can be achieved using the USB 4000 fiber optic spectrometer (Ocean Optics).

3 Results and discussion

The crystal structure of the $\text{Sr}_3\text{LaNb}_3\text{O}_{12}$ phosphor is shown in Fig. 1. It indicates that M (M = Nb/Sr/La) ions occupy a $3a$ lattice site in the proportion of 14% La, 28% Sr, and 58% Nb. M coordinating with six O ions at the position $3a$ lattice site forms the group, which is a regular octahedral biconical whose M–O distance is 1.91 Å. In the standard data, the cell parameters of the $\text{Sr}_3\text{LaNb}_3\text{O}_{12}$ are $a = b = 5.6590$ Å,

$c = 27.1780$ Å, $a/c = 0.2082$ Å, $V = 753.8$ Å³, and $Z = 3$.

The standard (PDF#00–041–0148) card of the $\text{Sr}_3\text{LaNb}_3\text{O}_{12}$ and eight XRD patterns of the $\text{Sr}_3\text{LaNb}_3\text{O}_{12}:x\text{Dy}^{3+}$ ($x = 0.01$ – 0.30 mol) samples are represented in Fig. 2a. The peaks of XRD have very narrow diffraction and show no evident mismatched peaks, which proves that the $\text{Sr}_3\text{LaNb}_3\text{O}_{12}:x\text{Dy}^{3+}$ ($x = 0.01$ – 0.30 mol) samples were successfully synthesized, and these phosphors are high phase purity. Using the substitution formula of the Dy^{3+} can calculate the substitution of the host lattices [28, 29]:

$$D_r = \frac{R_s(\text{CN}) - R_d(\text{CN})}{R_s(\text{CN})} \times 100\%, \quad (1)$$

where R_s is represented for the radius of the substituted cation, CN is on behalf of the coordination number, and D_r stands for the difference between the radius percentage, R_d represents the radius of the doped ions. The radius of Sr^{2+} ions is 1.180 Å and the radius of Nb^{3+} is 0.720 Å, whose D_r is 22.71% and -26.67%. But the radius of Dy^{3+} ions is 0.912 Å and its D_r is 11.62% which is the smallest and far less than 30%. Dy^{3+} ions and La^{3+} ions stay in the uniform valence state. The results indicate that the Dy^{3+} ion prefers to replace the La^{3+} ion. So The Dy^{3+} can quickly get into the host lattice, and it has no evident effect on the $\text{Sr}_3\text{LaNb}_3\text{O}_{12}$ crystal system.

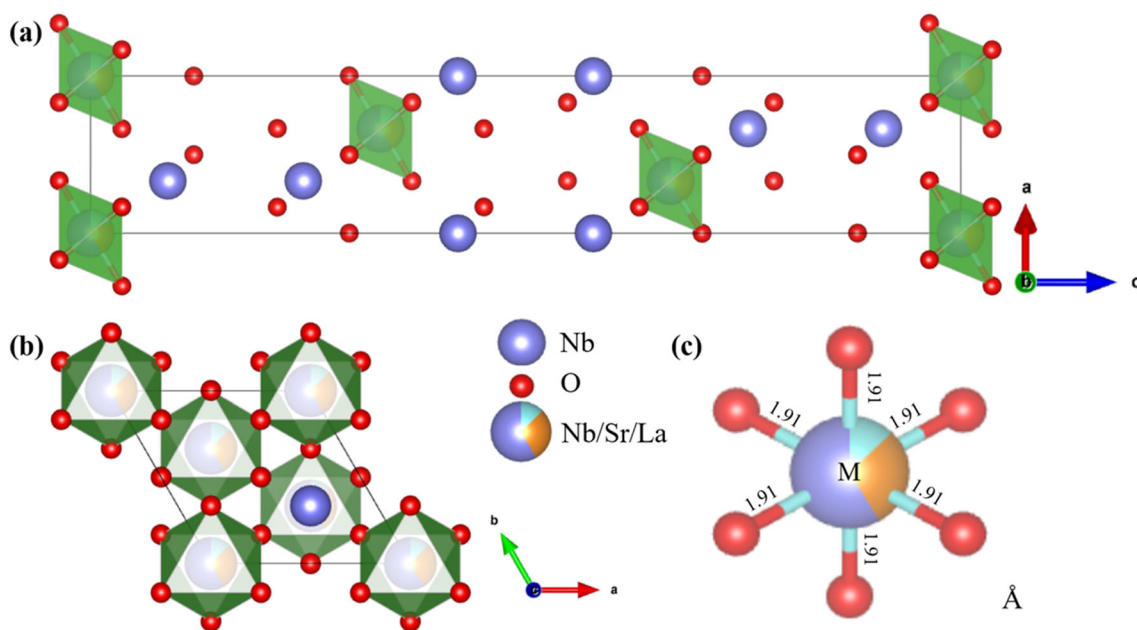


Fig. 1 a, b The crystal structure of the $\text{Sr}_3\text{LaNb}_3\text{O}_{12}$, c the coordination environment of M (Nb, Sr, and La)

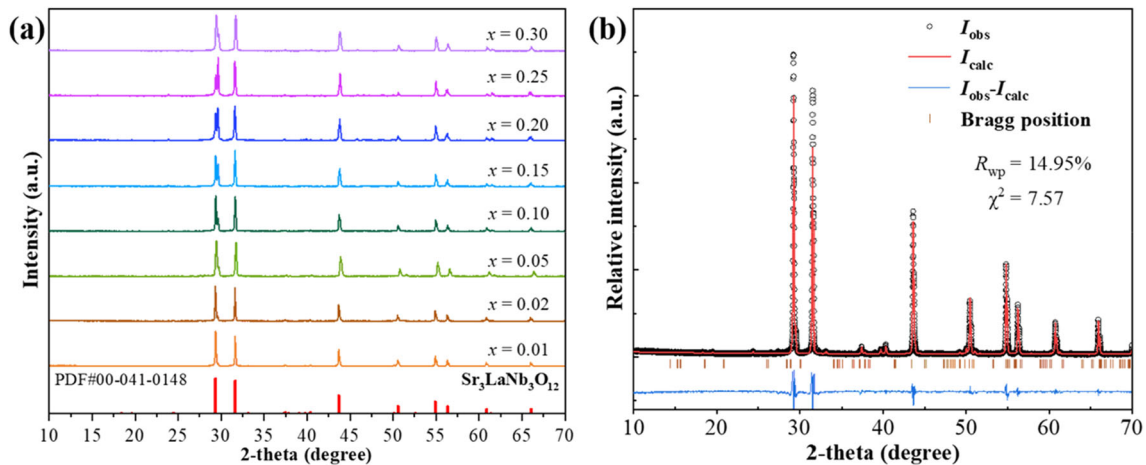


Fig. 2 **a** The XRD patterns of the $\text{Sr}_3\text{LaNb}_3\text{O}_{12}:x\text{Dy}^{3+}$ ($x = 0.01\text{--}0.30$ mol) phosphors, **b** Rietveld refinement results of the $\text{Sr}_3\text{LaNb}_3\text{O}_{12}:0.01\text{Dy}^{3+}$

In the Fig. 2b, the Rietveld refinement of the $\text{Sr}_3\text{LaNb}_3\text{O}_{12}:0.01\text{Dy}^{3+}$ phosphor was researched by using Maud software [30]. In Tables 1 and 2, the crystal structure parameters and Rietveld refinement data are shown. The lattice parameters of the $\text{Sr}_3\text{LaNb}_3\text{O}_{12}:0.01\text{Dy}^{3+}$ sample is $a = b = 5.65 \text{ \AA}$, $c = 27.19 \text{ \AA}$, $a/c = 0.2078$, $V = 753.28 \text{ \AA}^3$, and $Z = 3$. The obtained fitting parameters of $\text{Sr}_3\text{LaNb}_3\text{O}_{12}:0.01\text{Dy}^{3+}$ sample are $R_{\text{wp}} = 14.95\%$ and $\chi^2 = 7.57$, which indicates that the Dy^{3+} ions well replace La^{3+} ions in the $\text{Sr}_3\text{LaNb}_3\text{O}_{12}$ phosphors.

The surface morphology and size of phosphor is also necessary to study the use of w-LEDs. Figure 3a indicates SEM image of the $\text{Sr}_3\text{LaNb}_3\text{O}_{12}:0.01\text{Dy}^{3+}$ phosphor at 2400 magnification. The products are large conglomerations due to a high-temperature process. Figure 3b shows the particle size distribution of phosphor. $D(50)$ is 24.418 \mu m , which represents that 50% of the particles were less than 24.418 \mu m . $D(90)$ is 68.662 \mu m , which represents that 90% of the particles were less than 68.662 \mu m . The particle size

Table 1 The cell parameters of the $\text{Sr}_3\text{LaNb}_3\text{O}_{12}:0.01\text{Dy}^{3+}$ phosphor

Formula	Atom	x	y	z	Occ
$\text{Sr}_3\text{LaNb}_3\text{O}_{12}$	Nb1	0	0	0.4222	1
	Nb2	0	0	0	0.14
	Sr	0	0	0	0.28
	La	0	0	0	0.58
	O1	0.1670	0.3340	0.0360	1
	O2	0.1670	0.3340	0.4520	1

Table 2 The Rietveld refinement data of the $\text{Sr}_3\text{LaNb}_3\text{O}_{12}:0.01\text{Dy}^{3+}$ phosphor

Formula	$\text{Sr}_3\text{LaNb}_3\text{O}_{12}:0.01\text{Dy}^{3+}$
Crystal symmetry	Hexagonal
Space group	$R_{\bar{3}m}$ (trigonal)
Cell parameters	$a = b = 5.65 \text{ \AA}$ $c = 27.19 \text{ \AA}$ $\alpha = \beta = 90^\circ$ $\gamma = 120^\circ$ $Z = 3$
Cell Volume	753.28 \AA^3
R_{wp}	14.95%
χ^2	7.57

distribution of 22.556 \mu m is the largest cell volume percentage, which describes that they are suitable for use in solid-state lighting.

To confirm the elemental composition of samples, the type of the element can be analyzed using the EDS spectrum. By the EDS spectrum of the $\text{Sr}_3\text{LaNb}_3\text{O}_{12}:\text{Dy}^{3+}$ phosphor, all the elemental peaks can be observed containing Sr, La, Nb, O, and Dy. Figure 4b–g shows all the elements were even distribution. The weight percentages of the elements Sr, La, Nb, O and Dy are 29.27%, 16.74%, 31.34%, 22.29%, and 0.36%. The atomic percentages are 15.27%, 5.51%, 15.42%, 63.70%, and 0.10%. The results were consistent with the outcome of $\text{Sr}_3\text{LaNb}_3\text{O}_{12}:0.01\text{Dy}^{3+}$ phosphors. These proved that we successfully made the $\text{Sr}_3\text{LaNb}_3\text{O}_{12}:\text{Dy}^{3+}$ phosphors.

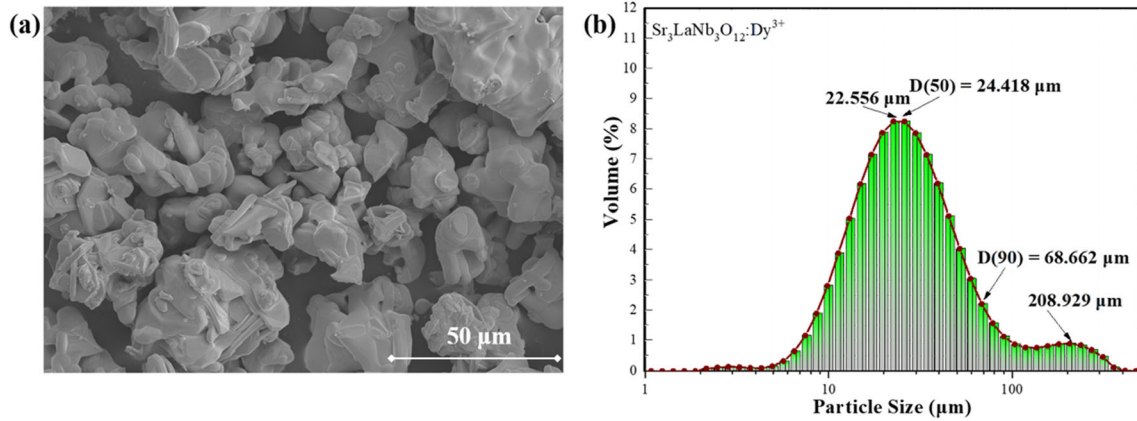


Fig. 3 a The SEM image of the $\text{Sr}_3\text{LaNb}_3\text{O}_{12}:0.01\text{Dy}^{3+}$, b the particle distribution of the $\text{Sr}_3\text{LaNb}_3\text{O}_{12}:0.01\text{Dy}^{3+}$

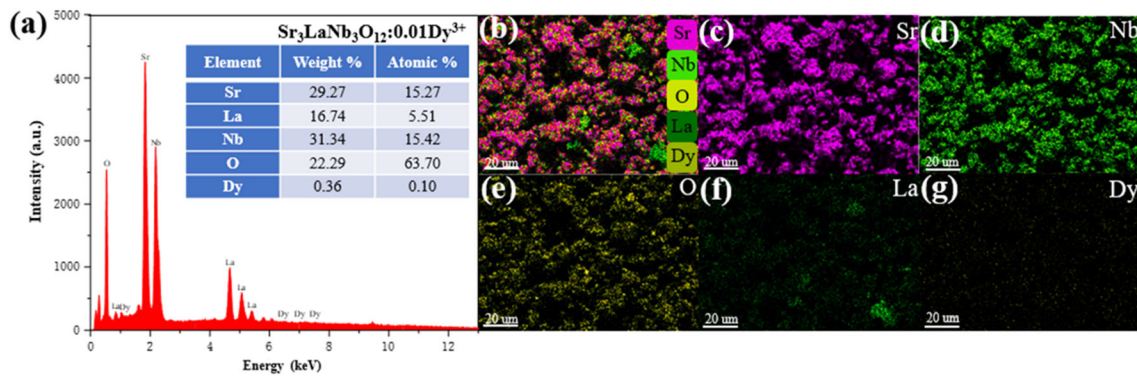


Fig. 4 a EDS spectrum and b–g elemental mapping of Sr, Nb, O, La, and Dy of the $\text{Sr}_3\text{LaNb}_3\text{O}_{12}:0.01\text{Dy}^{3+}$ phosphor

The excitation spectrum of the $\text{Sr}_3\text{LaNb}_3\text{O}_{12}:0.05\text{Dy}^{3+}$ is shown in Fig. 5a ($\lambda_{\text{em}} = 575 \text{ nm}$). The $\text{O}^{2-} - \text{Dy}^{3+}$ charge transfer (CT) causes a weak broad band ranging from 240 to 310 nm [31]. In the 300–500 nm

excitation spectrum, the seven remarkable peaks lie in 326, 352, 366, 388, 426, 454, and 475 nm, corresponding to the transition of the ${}^6\text{H}_{15/2}$ level to the ${}^6\text{P}_{3/2}$, ${}^6\text{P}_{7/2}$, ${}^6\text{P}_{5/2}$, ${}^4\text{I}_{13/2}$, ${}^4\text{G}_{11/2}$, ${}^4\text{I}_{15/2}$, and ${}^4\text{F}_{9/2}$ level

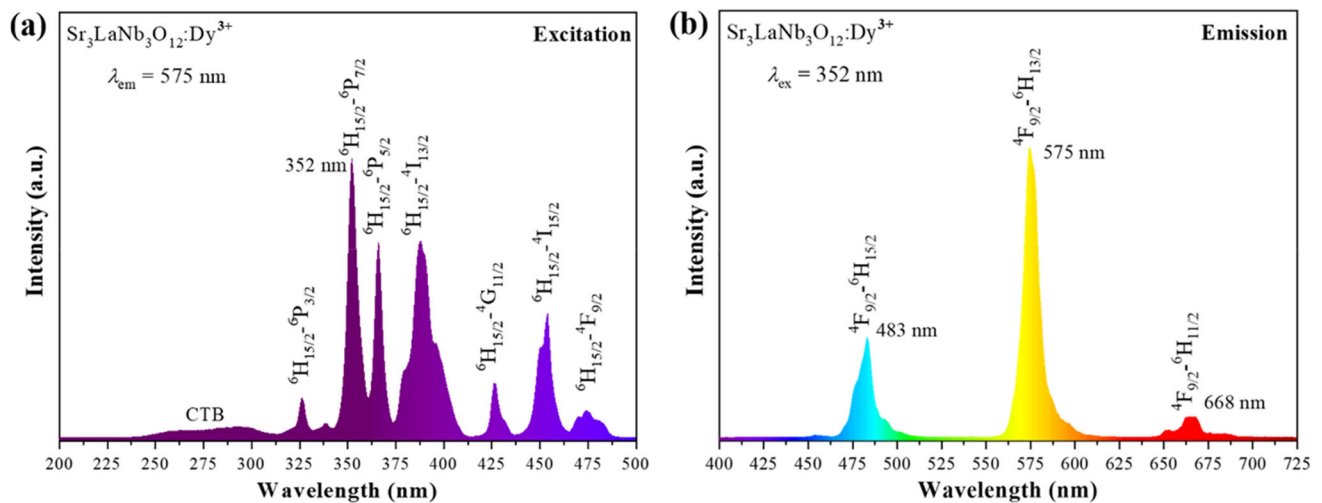


Fig. 5 a The excitation spectrum of the $\text{Sr}_3\text{LaNb}_3\text{O}_{12}:0.05\text{Dy}^{3+}$ ($\lambda_{\text{em}} = 575 \text{ nm}$), b The emission spectrum of the $\text{Sr}_3\text{LaNb}_3\text{O}_{12}:0.05\text{Dy}^{3+}$ ($\lambda_{\text{ex}} = 352 \text{ nm}$)

[32, 33]. Among these excitation peaks, the 352 nm excitation is the most favorable wavelength because of the Dy^{3+} transition (${}^6\text{H}_{15/2}$ - ${}^6\text{P}_{7/2}$), which will be suitable for the development of the n-UV-based w-LEDs.

Figure 5b describes the emission spectrum of $\text{Sr}_3\text{LaNb}_3\text{O}_{12}:0.05\text{Dy}^{3+}$ under the 352 nm excitation, delegated the three prominent emission peaks at 483 nm (${}^4\text{F}_{9/2}$ - ${}^6\text{H}_{15/2}$), 575 nm (${}^4\text{F}_{9/2}$ - ${}^6\text{H}_{13/2}$), and 668 nm (${}^4\text{F}_{9/2}$ - ${}^6\text{H}_{11/2}$). The most substantial peak was the yellow emission (${}^4\text{F}_{9/2}$ - ${}^6\text{H}_{13/2}$), but it was easily impacted by the external coordination environment, which is ascribed to the pure electric dipole transition. In contrast, the lower peak was the blue emission (${}^4\text{F}_{9/2}$ - ${}^6\text{H}_{13/2}$), which was not affected by the crystal field. The blue area (483 nm) of Dy^{3+} ions was lower than the yellow emission (575 nm) [34]. This phenomenon was identified with the fact that the Dy^{3+} ions occupied a lower symmetrical position.

To study the relationship between the doped Dy^{3+} concentration and the emission intensities, the emission spectra ($\lambda_{\text{ex}} = 352$ nm) of the $\text{Sr}_3\text{LaNb}_3\text{O}_{12}:x\text{Dy}^{3+}$ phosphors ($x = 0.01$ – 0.30 mol) were shown in Fig. 6a. Figure 6b clearly describes the relationship between the doping concentration of Dy^{3+} and the peak intensity of $\text{Sr}_3\text{LaNb}_3\text{O}_{12}:x\text{Dy}^{3+}$ by normalizing the maximum emission intensity. At the low doping concentration of Dy^{3+} ions, the luminous intensities gradually rises till the distance of centers reaches the critical distance where the optimal doping concentration was 0.05 mol in the $\text{Sr}_3\text{LaNb}_3\text{O}_{12}:\text{Dy}^{3+}$. After this point, the luminescence intensity presents the trend of falling, and the energy transfer ability has weakened. Figure 6c indicates the corresponding energy level schemes of the Dy^{3+} . Under the excitation of 352 nm, electrons are firstly transmitted from the ground state ${}^6\text{H}_{15/2}$ level to the higher excited state ${}^4\text{I}_{15/2}$ level. Then the excited electrons go through the non-radiative (NR) transition to ${}^4\text{F}_{9/2}$ level. In the end, the typical radiative transitions ${}^4\text{F}_{9/2}$ to ${}^6\text{H}_{M/2}$ ($M = 15, 13,$ and 11) of Dy^{3+} ions by can be observed, corresponding to the blue peak at 483 nm, the yellow main peak at 575 nm, and the red peak at 668 nm. Meanwhile, this process quickly releases the energy of phosphors through the non-radioactive transition.

To study the interaction mechanism between Dy^{3+} ions, the critical distance (R_c) is calculated. The value of the R_c is calculated by the subsequent formula [35, 36]:

$$R_c \approx 2 \left[\frac{3V}{4\pi X_c N} \right]^{\frac{1}{3}}, \quad (2)$$

where N is the number of cations, X_c is the optimal Dy^{3+} -doped concentration of the $\text{Sr}_3\text{LaNb}_3\text{O}_{12}$, and V is the volume of the cell. By substituting the value of X_c (0.05 mol), V (752.11 \AA^3), and N (3), the energy transfer distance can be calculated (21.25 \AA), which is far larger than the critical distance (5 \AA) of exchange. Therefore, the concentration quenching (CQ) is caused by the multipole-multipole interaction.

To further explore the connection between the Dy^{3+} -doping concentration and the luminous intensity, Dexter's model can be used. Dexter's model established the energy transfer between the same kinds of activators. On the basis of Dexter's theory, the specific role of the multipole energy transfer mechanism can be explored [37, 38]:

$$\frac{I}{x} = K \left[1 + \beta(x)^{\frac{\alpha}{3}} \right]^{-1}, \quad (3)$$

where I stands for emission intensity of different Dy^{3+} concentrations; x is the Dy^{3+} concentration; β and K are constants at a certain excitation wavelength in the same system. α represents a multipole interaction constant including three types of mechanism interaction: dipole–dipole, dipole–quadrupole, and quadrupole–quadrupole, corresponding to the $\alpha = 6, 8,$ and 10 . Figure 6d shows that the connection with x and I/x has a negative correlation relation, and the slope is determinately -1.81 . So the value of α is 5.43 , which is close to 6 . Therefore, the combined action of dipole–dipole causes the CQ of the Dy^{3+} -doped $\text{Sr}_3\text{LaNb}_3\text{O}_{12}$ phosphors.

The intensity of ${}^4\text{F}_{9/2}$ - ${}^6\text{H}_{15/2}$ and ${}^4\text{F}_{9/2}$ - ${}^6\text{H}_{13/2}$ transition at different concentrations is shown in Fig. 7. ${}^4\text{F}_{9/2}$ - ${}^6\text{H}_{15/2}$ represents the magnetic dipole (MD) transition, and ${}^4\text{F}_{9/2}$ - ${}^6\text{H}_{13/2}$ transition denotes the electric dipole (ED) transition. ED intensity is affected by the ligand ions in the crystal field [39]. The intensity of MD transition is weaker than the ED, which states that Dy^{3+} occupies the low symmetry site in the $\text{Sr}_3\text{LaNb}_3\text{O}_{12}$ matrix. Here, the asymmetric ratio ED/MD (R) play an important role in analyzing the symmetry of the lattice environment around Dy^{3+} . The R by calculating is $3.27, 3.00, 2.93, 2.77, 2.60, 2.42, 2.11,$ and 3.19 , corresponding to $x = 0.01, 0.02, 0.05, 0.10, 0.15, 0.20, 0.25,$ and 0.30 , respectively. The R of $\text{Sr}_3\text{LaNb}_3\text{O}_{12}:x\text{Dy}^{3+}$ ($x = 0.01$ – 0.30 mol)

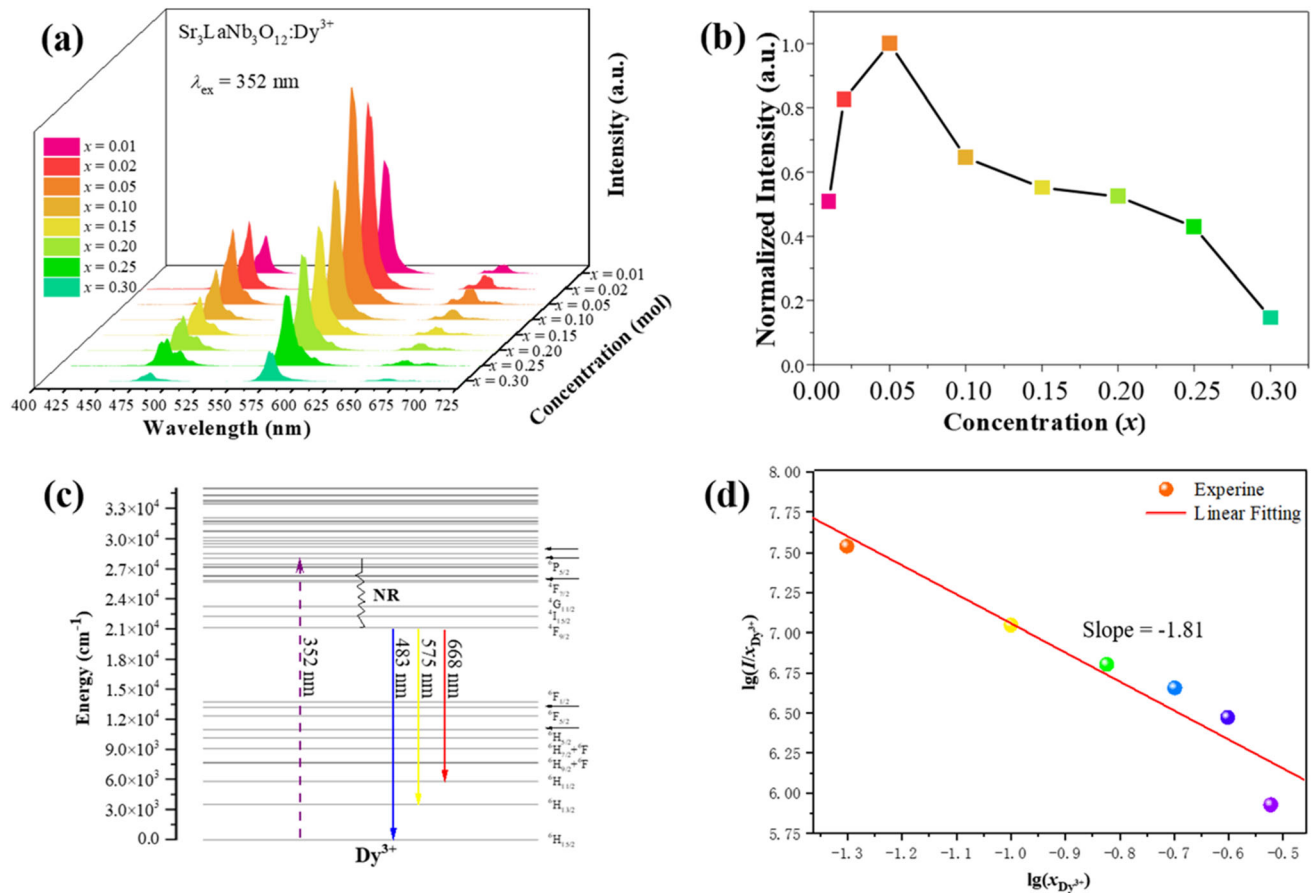


Fig. 6 **a** The PL emission of the $\text{Sr}_3\text{LaNb}_3\text{O}_{12}:\text{x}\text{Dy}^{3+}$ ($x = 0.01\text{--}0.30$ mol) at 352 nm, **b** The relationship between the doping concentrations of Dy^{3+} and the peak intensities of

$\text{Sr}_3\text{LaNb}_3\text{O}_{12}:\text{x}\text{Dy}^{3+}$, **c** The energy electron transition processes of Dy^{3+} levels diagram, **d** The relationship between $\lg(I/x)$ and $\lg(x)$ in the $\text{Sr}_3\text{LaNb}_3\text{O}_{12}:\text{Dy}^{3+}$ samples

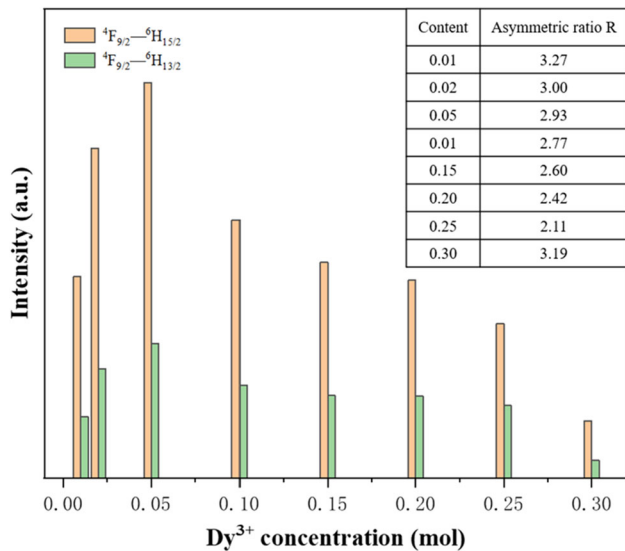


Fig. 7 The intensity of ${}^4\text{F}_{9/2}\text{--}{}^6\text{H}_{15/2}$ and ${}^4\text{F}_{9/2}\text{--}{}^6\text{H}_{13/2}$ transition at different concentrations

phosphors is greater than 1, which explains that Dy^{3+} ion occupied inversion symmetric lattice sites in the $\text{Sr}_3\text{LaNb}_3\text{O}_{12}$ crystal structure [40].

Thermal stability plays an important role that is analyzed to decide whether the phosphors are suitable for the w-LED application. When the LED chip temperature can reach about 420 K, excellent phosphors can sustain high temperatures and against a color shift. As follows, the effect of changing temperature in the range of 300–480 K on the luminescent intensity of the $\text{Sr}_3\text{LaNb}_3\text{O}_{12}:0.02\text{Dy}^{3+}$ and $\text{Sr}_3\text{LaNb}_3\text{O}_{12}:0.05\text{Dy}^{3+}$ were also studied in Fig. 8a, b. The emission intensity rise and then fall when the temperature increase but the emission peaks of both phosphors hardly shift. It can also be observed through the normalized integral emission intensity. Figure 8c, d clearly plots the normalized integrated PL intensities versus temperature for representative samples. It engenders thermal quenching, and

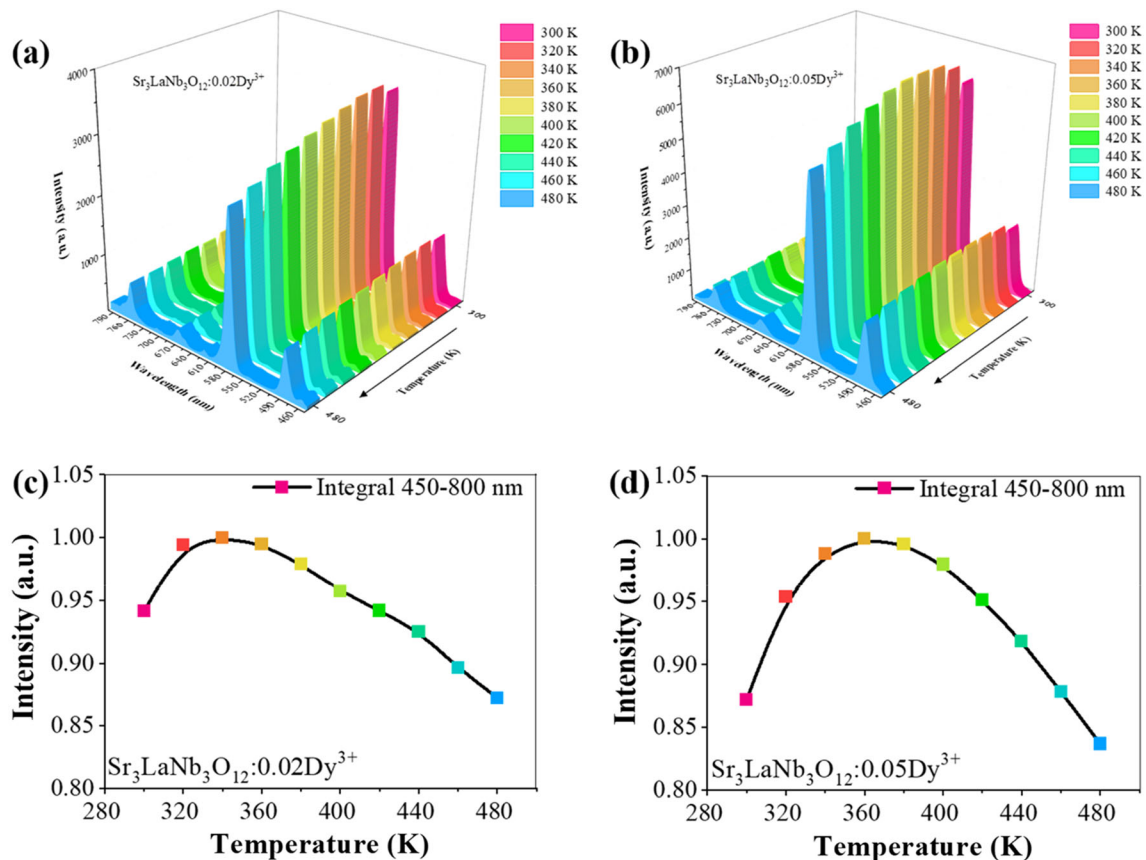


Fig. 8 (a, b) and (c, d) of the temperature-dependent emission spectra of the $\text{Sr}_3\text{LaNb}_3\text{O}_{12}:0.02\text{Dy}^{3+}$ and $\text{Sr}_3\text{LaNb}_3\text{O}_{12}:0.05\text{Dy}^{3+}$, and the emission intensity of the $\text{Sr}_3\text{LaNb}_3\text{O}_{12}:0.02\text{Dy}^{3+}$ and $\text{Sr}_3\text{LaNb}_3\text{O}_{12}:0.05\text{Dy}^{3+}$

compared with the luminous intensity of the initial temperature, the intensity of 480 K has not obviously fallen. For the $\text{Sr}_3\text{LaNb}_3\text{O}_{12}:0.02\text{Dy}^{3+}$ phosphor, the PL intensity increased abnormally by approximately 6% from 300 to 340 K. For the $\text{Sr}_3\text{LaNb}_3\text{O}_{12}:0.05\text{Dy}^{3+}$ phosphor, the PL intensity increased abnormally by approximately 13% from 300 to 360 K. Then the intensities of the both phosphors decreased with the further increase in temperature.

The phosphor exhibited abnormal thermal quenching, first discovered in $\text{Na}_3\text{Sc}_2(\text{PO}_4)_3:\text{Eu}^{2+}$ blue phosphors in 2017 [41]. It was later found in several phosphors [42–46]. In the $\text{Sr}_3\text{LaNb}_3\text{O}_{12}$ crystal, Sr, La, and Nb ions occupy the same crystal sites. Moreover, the radius of Sr^{2+} ($r = 1.18 \text{ \AA}$, CN = 6) is very close to that of Dy^{3+} ($r = 0.912 \text{ \AA}$, CN = 6). Dy^{3+} may enter into the Sr^{2+} lattice of $\text{Sr}_3\text{LaNb}_3\text{O}_{12}$, an unbalanced charge substitution causing lattice defects [47]. Therefore, this abnormal thermal quenching phenomenon can ascribe to the lattice defects, which function like electron capture centers.

In the end, the remaining energy of the excited electron was transferred and stored in Dy^{3+} , which was higher than the loss caused by NR transition. Therefore, the emission intensity became stronger as temperature increased. It showed good thermal stability and potential in high-power photoelectric devices, especially w-LEDs.

Besides the variation of emission spectral intensity, the change of CIE chromaticity coordinates can also be used to evaluate the stability of phosphors at different temperatures. The CIE chromaticity coordinates of the $\text{Sr}_3\text{LaNb}_3\text{O}_{12}:0.02\text{Dy}^{3+}$ and $\text{Sr}_3\text{LaNb}_3\text{O}_{12}:0.05\text{Dy}^{3+}$ vary only slightly from 300 to 480 K in Fig. 9a, b. Therefore, the phosphors are almost the same color. The changes in CIE chromaticity coordinates of the $\text{Sr}_3\text{LaNb}_3\text{O}_{12}:0.02\text{Dy}^{3+}$ and $\text{Sr}_3\text{LaNb}_3\text{O}_{12}:0.05\text{Dy}^{3+}$, respectively are ($\Delta x = 3.89 \times 10^{-5}$, $\Delta y = 6.94 \times 10^{-5}$) and ($\Delta x = 3.33 \times 10^{-6}$, $\Delta y = 0.89 \times 10^{-5}$) by calculating. So the phosphors manifest good coloring stability at high temperatures.

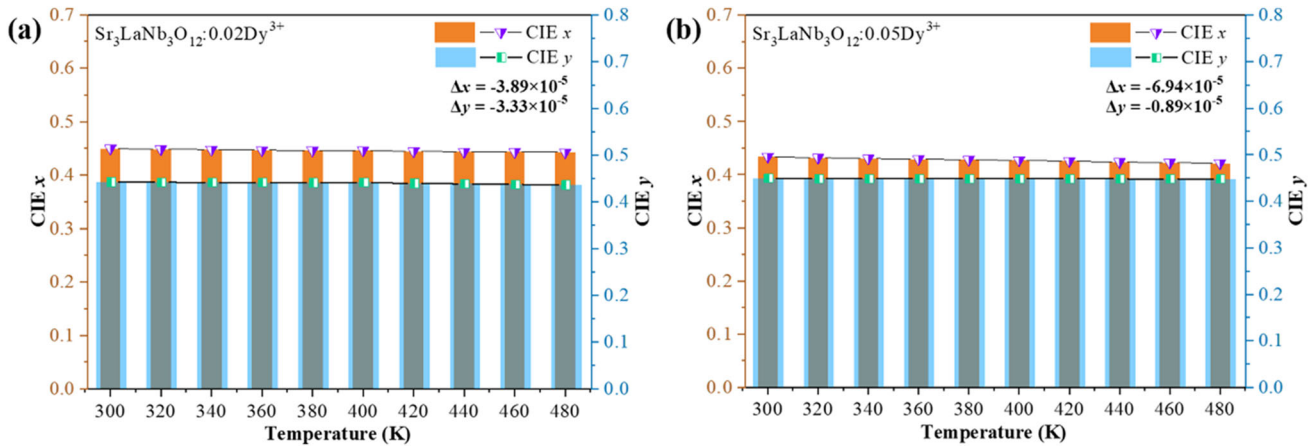


Fig. 9 a, b Chromaticity coordinates at different temperatures of the $\text{Sr}_3\text{LaNb}_3\text{O}_{12}:0.02\text{Dy}^{3+}$ and $\text{Sr}_3\text{LaNb}_3\text{O}_{12}:0.05\text{Dy}^{3+}$

For the sake of learning the mechanism of thermal quenching, the research knows more about the activation energy (E_a) of thermal quenching. By the Arrhenius model combined with experimental data, the relational graph of $\ln[(I_0/I) - 1] \sim 1/T$ was used to achieve the activation energy in Fig. 10. The following is the Arrhenius equation [48–50]:

$$I(T) = \frac{I_0}{1 + c \exp(-E_a/kT)}, \tag{4}$$

where I_0 is the initial luminous intensity; k is a Boltzmann constant, which is 8.62×10^{-5} eV/K; $I(T)$ is the luminous intensity in different temperatures; c is a constant; E_a is the constant activation energy. The calculated E_a of the $\text{Sr}_3\text{LaNb}_3\text{O}_{12}:\text{Dy}^{3+}$ was 0.29 eV, which further indicated that the $\text{Sr}_3\text{LaNb}_3\text{O}_{12}:\text{xDy}^{3+}$ have good thermal stability.

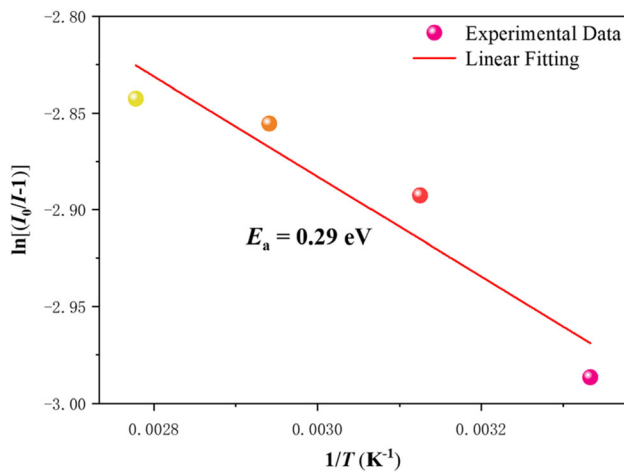


Fig. 10 The relevance of $\ln [(I_0/I) - 1]$ versus $1/T$

CIE chromaticity coordinates play an important role in evaluating the luminescence properties of the phosphors. The CIE chromaticity coordinates of the $\text{Sr}_3\text{LaNb}_3\text{O}_{12}:\text{xDy}^{3+}$ ($x = 0.01, 0.02, 0.05, 0.10, 0.15, 0.20, 0.25,$ and 0.30 mol) phosphor samples namely are (0.426, 0.452), (0.420, 0.448), (0.425, 0.450), (0.421, 0.449), (0.424, 0.446), (0.422, 0.442), (0.416, 0.434), and (0.435, 0.455), respectively, as listed in Table 3. The CIE chromaticity coordinates of the $\text{Sr}_3\text{LaNb}_3\text{O}_{12}:\text{xDy}^{3+}$ ($x = 0.01\text{--}0.30$ mol) samples are shown in Fig. 11. They all drop into the yellow-light region of the CIE 1931 chromaticity coordinates, and all points are distributed in one piece. In addition, with increasing doping concentration, the CIE chromaticity coordinates (x, y) show a little change, and the chromaticity coordinate displacement ($\Delta x, \Delta y$) is (0.019, 0.022). The small change indicate the different Dy^{3+} -doped concentrations do not make a difference in color. The data indicated that the $\text{Sr}_3\text{LaNb}_3\text{O}_{12}:\text{xDy}^{3+}$ ($x = 0.01\text{--}0.30$ mol) phosphors have good color stability to apply in w-LEDs.

Table 3 The CIE color coordinates and CCT of the $\text{Sr}_3\text{LaNb}_3\text{O}_{12}:\text{xDy}^{3+}$ ($x = 0.01\text{--}0.30$ mol) phosphors

Concentration x (mol)	Chromaticity coordinates	CCT (K)
0.01	(0.426, 0.452)	3245
0.02	(0.420, 0.448)	3375
0.05	(0.425, 0.450)	3252
0.10	(0.421, 0.449)	3346
0.15	(0.424, 0.446)	3258
0.20	(0.422, 0.442)	3271
0.25	(0.416, 0.434)	3275
0.30	(0.435, 0.455)	3242

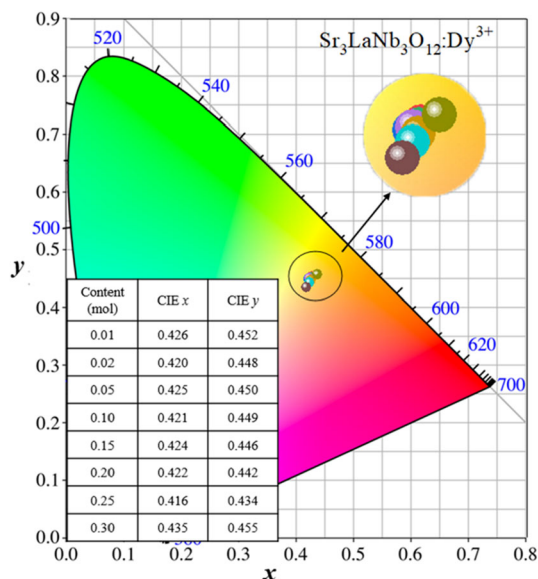


Fig. 11 CIE chromaticity coordinates for the prepared $\text{Sr}_3\text{LaNb}_3\text{O}_{12}:\text{x}\text{Dy}^{3+}$ ($x = 0.01\text{--}0.30$ mol) samples

CCT is also important for the luminescence properties of phosphors. The CCT value affects whether the lamp emits warm or cold light. The light shows a cold lamp when CCT is more significant than 4000 K, the light emits a warm lamp while CCT is less than 3200 K. By the McCamy formula, CCT can be calculated [51, 52]:

$$\text{CCT} = -449n^3 + 3525n^2 - 6823n + 5520.33, \quad (5)$$

where inverse slope line, $n = (x-x_e)/(y-y_e)$, (x, y) are the chromaticity coordinates of the $\text{Sr}_3\text{LaNb}_3\text{O}_{12}:\text{x}\text{Dy}^{3+}$ ($x = 0.01\text{--}0.30$ mol) samples, and (x_e, y_e) are the coordinates of the epicenter, which are (0.332, 0.186). The CCT value corresponding to the $\text{Sr}_3\text{LaNb}_3\text{O}_{12}:\text{x}\text{Dy}^{3+}$ ($x = 0.01\text{--}0.30$ mol) phosphors can be calculated in Table 2. These CCTs correspond to 3245, 3375, 3252, 3346, 3258, 3271, 3275, and 3242 K, respectively, which prove that these phosphors could be applied in w-LEDs.

The QY play an important role in w-LED application, which is calculated by the following equation [53]:

$$\eta_{\text{QY}} = \frac{\int L_s}{\int E_R - \int E_s}, \quad (6)$$

where L_s is the emission spectrum of the $\text{Sr}_3\text{LaNb}_3\text{O}_{12}:\text{0.05}\text{Dy}^{3+}$, E_s and E_R represent the excitation light with and without the sample in the integrating sphere, respectively. The calculating QY value of the $\text{Sr}_3\text{LaNb}_3\text{O}_{12}:\text{0.05}\text{Dy}^{3+}$ phosphor is 18.24% under

352 nm in Fig. 12, which shows that the $\text{Sr}_3\text{LaNb}_3\text{O}_{12}:\text{0.05}\text{Dy}^{3+}$ phosphor is suitable for application for w-LEDs.

The synthesized $\text{Sr}_3\text{LaNb}_3\text{O}_{12}:\text{0.05}\text{Dy}^{3+}$ yellow phosphor, BAM blue phosphor, and (Sr, Ca)AlSiN₃:Eu²⁺ red phosphor were combined with the n-UV InGaN chip (388 nm) to make up a w-LED. The prepared w-LED has high R_a (91), low CCT (4162 K), and CIE coordinates (0.365, 0.368). Figure 13a reveals that the manufactured w-LED compares with the commercial w-LED in terms of CRI values. R_a plays a vital role in describing a parameter of the w-LED luminescence properties. The histogram comparison of the particular rendering index ($R_1\text{--}R_{14}$) shows the rendering performance of different colors. It is significantly higher than the commercial w-LED values ($R_a = 80$, $R_9 = 15$) [54–56]. Thus, a new component phosphor is used to produce w-LED to make up for the traditional limitations and has excellent potential in the future. Figure 13b shows the CIE coordinates for preparing the w-LED, which is lying white area and approaching the equal-energy point coordinates (0.333, 0.333). Therefore, this w-LED can become an excellent alternative to commercial w-LEDs.

4 Conclusions

In summary, the $\text{Sr}_3\text{LaNb}_3\text{O}_{12}:\text{x}\text{Dy}^{3+}$ ($x = 0.01\text{--}0.30$ mol) of space group R_{3m} perovskite was successfully synthesized by high-temperature solid-phase method. The XRD patterns proved that the

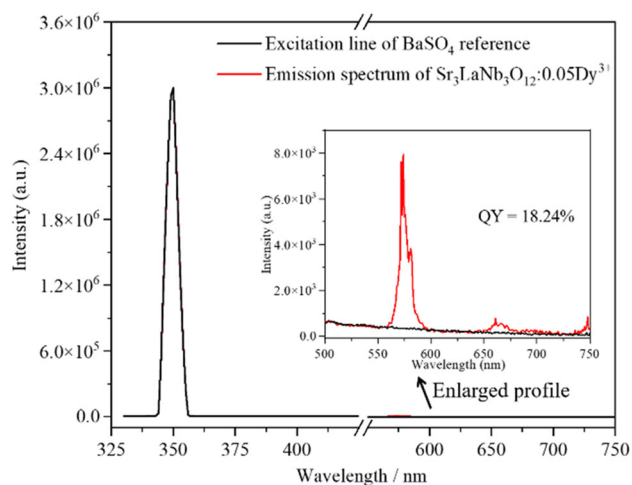


Fig. 12 QY for the $\text{Sr}_3\text{LaNb}_3\text{O}_{12}:\text{0.05}\text{Dy}^{3+}$

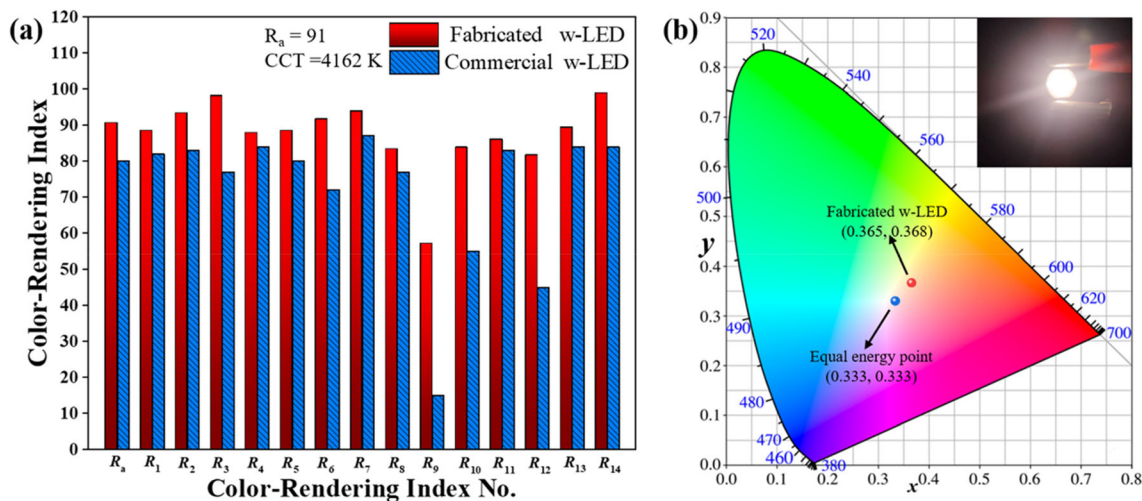


Fig. 13 **a** A comparison of the prepared w-LED and the commercial w-LED in color rendering index (CRI), **b** The CIE coordinates of w-LED at a forward-bias current of 300 mA

prepared $\text{Sr}_3\text{LaNb}_3\text{O}_{12}:x\text{Dy}^{3+}$ ($x = 0.01\text{--}0.30$ mol) phosphors were a pure phase, and the Dy^{3+} ions can quickly replace the La^{3+} ions which has no effect on the crystal structure. The element distribution maps of the prepared samples are distributed. $\text{Sr}_3\text{LaNb}_3\text{O}_{12}:0.05\text{Dy}^{3+}$ had the most optimal luminescence intensity among a series of $\text{Sr}_3\text{LaNb}_3\text{O}_{12}$ doped with different concentrations of Dy^{3+} . Under the excitation of 352 nm, $\text{Sr}_3\text{LaNb}_3\text{O}_{12}:0.05\text{Dy}^{3+}$ had a prominent yellow peak of 575 nm, which was $^4\text{F}_{9/2}\text{--}^6\text{H}_{13/2}$. The observed CQ phenomenon was caused by the interaction of dipole–dipole. The abnormal thermal phenomenon was due to lattice defects where Dy^{3+} replaces Sr^{2+} . The activation energy of phosphor was calculated to be 0.29 eV. The CIE coordinates were located in the yellow region. The changes in temperature and doping concentration had only a slight effect on the color stability. White light with low CCT (4162 K) and R_a (91) was successfully prepared by an n-UV InGaN chip (388 nm), whose CIE chromaticity coordinates were (0.365, 0.368). $\text{Sr}_3\text{LaNb}_3\text{O}_{12}:\text{Dy}^{3+}$ was expected to replace commercial yellow phosphor in w-LED applications due to its high thermal stability and excellent optical performance.

Author contributions

All authors contributed to the study conception and design. Material preparation, data collection, and analysis were performed by Yuchen Zhang, Zhikai

Liang, Weixian Wang, Yifang Lin, Rong Tang, Jingfei Wang, Daomiao He, Jinhui Liu, Zhong Zhang, Lingzhi Zhao, Bin Deng, Dan Zhang, Ruijin Yu. The first draft of the manuscript was written by Yuchen Zhang and all authors commented on previous versions of the manuscript. All authors read and approved the final manuscript.

Funding

This work was supported by the Undergraduate Innovation Fund of Northwest A&F University, China (202210712058, 202210712050, S202210712394, 202110712190, 202110712188, S202110712707, S202010712314, S202010712006), the Scientific and Technological Plan of Guangdong Province, China (No. 2019B090905005), National Natural Science Foundation of China (No. 11804265), and Home for researchers (www.home-for-researchers.com), China.

Data availability

The data that support the findings of this study are available on request from the corresponding author. The data are not publicly available due to privacy or ethical restrictions.

Declarations

Conflict of interests I certify that the Yuchen Zhang and other co-authors of the article “Optical properties of yellow-emitting $\text{Sr}_3\text{LaNb}_3\text{O}_{12}:\text{Dy}^{3+}$ phosphors with an abnormal thermal quenching for w-LED applications” have no conflict of interest, financial or otherwise.

References

- G. Li, X. Lu, Q. Mao, G. Du, M. Liu, L. Chu, J. Zhong, Suppression of charge imbalance via $\text{Li}^+-\text{Mn}^{4+}$ co-incorporated Sr_2YSbO_6 red phosphors for warm w-LEDs. *Mater. Today Chem.* **23**, 100744 (2022)
- Y. Chen, Y.M. Lan, D. Wang, G.X. Zhang, W.L. Peng, Y.Q. Chen, X. He, Q.G. Zeng, J. Wang, Luminescence properties of $\text{Gd}_2\text{MoO}_6:\text{Eu}^{3+}$ nanophosphors for WLEDs. *Dalton T.* **50**, 6281–6289 (2021)
- Y.X. Cao, X.C. Wang, J.Y. Ding, X.P. Zhou, T. Seto, Y.H. Wang, Constructing a single-white-light emission by finely modulating the occupancy of luminescence centers in europium-doped $(\text{Ca}_{1-x}\text{Sr}_x)_9\text{Bi}(\text{PO}_4)_7$ for WLEDs. *J. Mater. Chem. C* **8**, 9576–9584 (2020)
- X.W. Li, H.L. Xu, X.M. Xia, F.Y. Xie, S.L. Zhong, D.K. Xu, One-step synthesis of $\text{Sc}_2\text{W}_3\text{O}_{12}:\text{Eu}^{3+}$ phosphors with tunable luminescence for WLED. *Ceram Int.* **45**, 10461–10467 (2019)
- M. Chen, H. Hu, N. Yao, X. Yuan, Q. Zhong, M. Cao, Y. Xu, Q. Zhang, Solvothermal synthesis of cesium lead halide nanocrystals with controllable dimensions: a stoichiometry defined growth mechanism. *J. Mater. Chem. C* **7**, 14493–14498 (2019)
- L. Ding, Y. Wang, P. Zhu, Y. Bai, One-step plant-inspired reaction that transform membrane hydrophobicity into high hydrophilicity and underwater super oleophobicity for oil-in-water emulsion separation. *Appl. Surf. Sci.* **479**, 423–429 (2019)
- H.M. Li, R. Pang, G.Y. Liu, W.Z. Sun, D. Li, L.H. Jiang, S. Zhang, C.Y. Li, J. Feng, H.J. Zhang, Synthesis and luminescence properties of Bi^{3+} -activated K_2MgGeO_4 : a promising high-brightness orange-emitting phosphor for WLEDs conversion. *Inorg Chem.* **57**, 12303–12311 (2018)
- J.H. Li, Z.H. Zhang, X.H. Li, Y.Q. Xu, Y.Y. Ai, J. Yan, J.X. Shi, M.M. Wu, Luminescence properties and energy transfer of $\text{YGa}_{1.5}\text{Al}_{1.5}(\text{BO}_3)_4$: Tb^{3+} , Eu^{3+} as a multi-colour emitting phosphor for WLEDs. *J. Mater. Chem. C* **5**, 6294–6299 (2017)
- G. Hu, Y. Sun, J. Zhuang, X. Zhang, H. Zhang, M. Zheng, Y. Xiao, Y. Liang, H. Dong, H. Hu, B. Lei, C. Hu, Y. Liu, Enhancement of fluorescence emission for tricolor quantum dots assembled in polysiloxane toward solar spectrum-simulated white light-emitting devices. *Small* **16**, e1905266 (2020)
- N. Schulte-Römer, J. Meier, M. Söding, E. Dannemann, The LED paradox: how light pollution challenges experts to reconsider sustainable lighting. *Sustainability.* **11**, 6060 (2019)
- L. Franke, D. Sülflow, K. Stark, H. Piazena, R. Uebelhack, Acute effect of blue light exposition on well-being and melatonin secretion in humans. *Eur. Psychiat.* **24**, 1–1 (2020)
- S. Thakur, R. Dhakal, P.K. Verkicharla, Short-term exposure to blue light shows an inhibitory effect on axial elongation in human eyes independent of defocus. *Invest. Ophthalm. Vis. Sci.* **62**, 22 (2021)
- Q. Wang, Z. Mu, L. Yang, S. Zhang, D. Zhu, Y. Yang, D. Luo, F. Wu, The synthesis and the luminescence properties of $\text{Sr}_2\text{Ga}_3\text{La}_{1-x}\text{Dy}_x\text{Ge}_3\text{O}_{14}$. *Physica. B* **530**, 258–263 (2018)
- Q. Wang, Z. Mu, S. Zhang, Q. Zhang, D. Zhu, J. Feng, Q. Du, F. Wu, A novel near infrared long-persistent phosphor $\text{La}_2\text{MgGeO}_6:\text{Cr}^{3+}$, RE^{3+} ($\text{RE} = \text{Dy}, \text{Sm}$). *J. Lumin.* **206**, 618–623 (2019)
- L. Yang, Z. Mu, S. Zhang, Q. Wang, D. Zhu, Y. Zhao, D. Luo, Q. Zhang, F. Wu, Dy^{3+} Doped $\text{Ca}_9\text{Gd}(\text{PO}_4)_7$: a novel single-phase full-color emitting phosphor. *J. Mater. Sci-Mater. El.* **29**, 6548–6555 (2018)
- L. Camargo, P.R. González, M. Santiago, H.O. Dávila, J. Marcazzó, A preliminary study of the radioluminescence and optically stimulated luminescence of $\text{CaF}_2:\text{Ce}, \text{Dy}$ phosphor. *J. Lumin.* **246**, 118845 (2022)
- H.Y. Wu, H.M. Li, L.H. Jiang, R. Pang, S. Zhang, D. Li, G.Y. Liu, C.Y. Li, J. Feng, H.J. Zhang, Synthesis, structure and optical properties of novel thermally robust Dy^{3+} -doped $\text{Ca}_9\text{Sc}(\text{PO}_4)_7$ phosphors for NUV-excited white LEDs. *J. Rare. Earth.* **39**, 277–283 (2021)
- L. Li, F. Qin, Y. Zhou, Y. Zheng, J. Miao, Z. Zhang, Photoluminescence and time-resolved-luminescence of $\text{CaWO}_4:\text{Dy}^{3+}$ phosphors. *J. Lumin.* **224**, 117308 (2020)
- X. Wu, X. Zhao, Q. Ren, L. Du, M. Pei, O. Hai, Tuning of emission by effect of local symmetry in $\text{BaLaLiWO}_6:\text{Dy}^{3+}/\text{Eu}^{3+}$ for WLEDs. *Ceram. Int.* **48**, 18793–18802 (2022)
- P. Vinodkumar, S. Panda, G. Jaiganesh, R.K. Padhi, U. Madhusoodanan, B.S. Panigrahi, SrBPO_5 : Ce^{3+} , Dy^{3+} - a cold white-light emitting phosphor. *Spectrochim. Acta. A* **253**, 119560 (2021)
- K. Dev, A. Selot, G.B. Nair, V.L. Barai, F.Z. Haque, M. Aynyas, S.J. Dhoble, Energy transfer from Ce^{3+} to Dy^{3+} ions for white light emission in $\text{Sr}_2\text{MgAl}_{22}\text{O}_{36}:\text{Ce}^{3+}$, Dy^{3+} phosphor. *J. Lumin.* **206**, 380–385 (2019)

22. P. Du, J.S. Yu, Photoluminescence, cathodoluminescence and thermal stability of Sm^{3+} -activated $\text{Sr}_3\text{La}(\text{VO}_4)_3$ red-emitting phosphors. *Luminescence* **32**, 1504–1510 (2017)
23. P. Sehrawat, R.K. Malik, R. Punia, S.P. Khatkar, V.B. Taxak, Augmenting the photoluminescence efficiency via enhanced energy-relocation of new white-emitting $\text{BaYAlZn}_3\text{O}_7$: Dy^{3+} nano-crystalline phosphors for WLEDs. *J. Alloy. Compd.* **879**, 160371 (2021)
24. L. Zhang, X. Zhang, C. Zhao, Crystal structure, luminescence properties and thermal stability of novel $\text{Sr}_2\text{CaLa}(\text{VO}_4)_3$: Sm^{3+} phosphor synthesized by the combustion method. *J. Alloy. Compd.* **899**, 163378 (2022)
25. M. Wang, X. Hu, Z. Zhan, T. Sun, Y. Tang, Facile fabrication of CeVO_4 hierarchical hollow microspheres with enhanced photocatalytic activity. *Mater. Lett.* **253**, 259–262 (2019)
26. T. Sun, M. Wang, Y. Tang, J. Ding, Y. Zhang, Copolymer-assisted synthesis and photoluminescent properties of 3D hierarchical EuF_3 spherical architectures. *Mater. Lett.* **177**, 120–123 (2016)
27. M. Wang, X. Yang, S. Tian, Y. Guo, T. Sun, M. Wang, Y. Tang, Constructing novel hierarchical porous hydrangea-like ZnWO_4 microspheres with enhanced photocatalytic performance. *Mater. Lett.* **264**, 127417 (2020)
28. F. Fan, L. Zhao, Y. Shang, J. Liu, W. Chen, Y. Li, Thermally stable double-perovskite Ca_3TeO_6 : Eu^{3+} red-emitting phosphors with high color purity. *J. Lumin.* **211**, 14–19 (2019)
29. P. Cai, L. Qin, C. Chen, J. Wang, S. Bi, S.I. Kim, Y. Huang, H.J. Seo, Optical thermometry based on vibration sidebands in Y_2MgTiO_6 : Mn^{4+} double perovskite. *Inorg. Chem.* **57**, 3073–3081 (2018)
30. C.X. Luo, Y.X. Zhang, T.F. Deng, Pressureless sintering of high performance silicon nitride ceramics at 1620 degrees C. *Ceram. Int.* **47**, 29371–29378 (2021)
31. K. Mishra, S.K. Singh, A.K. Singh, S.B. Rai, Optical characteristics and charge transfer band excitation of Dy^{3+} doped Y_2O_3 phosphor. *Mater Res Bull.* **47**, 1339–1344 (2012)
32. P. Dewangan, D.P. Bisen, N. Brahme, S. Sharma, R.K. Tamrakar, I.P. Sahu, K. Upadhyay, Influence of Dy^{3+} concentration on spectroscopic behaviour of $\text{Sr}_3\text{MgSi}_2\text{O}_8$: Dy^{3+} phosphors. *J. Alloy. Compd.* **816**, 152590 (2020)
33. B.C. Jamalaliah, Y.R. Babu, Near UV excited SrAl_2O_4 : Dy^{3+} phosphors for white LED applications. *Mater. Chem. Phys.* **211**, 181–191 (2018)
34. J.X. An, S. Zhang, R.W. Liu, G.X. Hu, Z.W. Zhang, Y.Y. Qiu, Y.Y. Zhou, F.M. Zeng, Z.M. Su, Luminescent properties of $\text{Dy}^{3+}/\text{Eu}^{3+}$ doped fluorescent glass for white LED based on oxyfluoride matrix. *J. Rare. Earth.* **39**, 26–32 (2021)
35. G.S.R. Raju, E. Pavitra, H. Patnam, G.L. Varaprasad, N.R. Chodankar, S.J. Patil, K.S. Ranjith, M.V.B. Rao, J.S. Yu, J.Y. Park, Y.S. Huh, Y.K. Han, Rationalized crystal structure augmented highly efficient far-red-emitting double perovskite niobate phosphor for indoor plant growth LED applications. *J. Alloy Compd.* **903**, 163881 (2022)
36. L. Tang, L. Zhou, X. Yan, K. Zhong, X. Gao, J. Li, A new NIR-emissive fluorescence turn-on probe for Hg^{2+} detection with a large Stokes shift and its multiple applications. *J. Photoch. Photobio. A* **387**, 112160 (2020)
37. Y. Tang, Y. Liu, W.M. Ning, L.S. Zhan, J.Q. Ding, M.L. Yu, H.J. Liu, Y.H. Gao, G.H. Xie, C.L. Yang, Manipulating Forster and Dexter interactions between a thermally activated delayed fluorescence host and a phosphorescent dopant for highly efficient solution-processed red and white OLEDs. *J. Mater. Chem. C* **10**, 4637 (2022)
38. G. Sowjanya, R. Doddaji, V.R.M. Reddy, Structural, luminescence, energy transfer mechanism, and photometric properties of Sm^{3+} -doped KYBO phosphors. *Radiat. Phys. Chem.* **190**, 109791 (2022)
39. M. Rajendran, S. Vaidyanathan, Zero-concentration quenching: a novel Eu^{3+} based red phosphor with non-layered crystal structure for white LEDs and $\text{NaSrY}(\text{MoO}_4)_3$: Sm^{3+} based deep-red LEDs for plant growth. *Dalton T.* **49**, 9239–9253 (2020)
40. A. Hooda, S.P. Khatkar, A. Khatkar, S. Chahar, S. Devi, J. Dalal, V.B. Taxak, Characteristic white light emission via down-conversion SrGdAlO_4 : Dy^{3+} nanophosphor. *Curr. Appl. Phys.* **19**, 621–628 (2019)
41. Y.H. Kim, P. Arunkumar, B.Y. Kim, S. Unithrattil, E. Kim, S.H. Moon, J.Y. Hyun, K.H. Kim, D. Lee, J.S. Lee, W.B. Im, A zero-thermal-quenching phosphor. *Nat. Mater.* **16**, 543–550 (2017)
42. Y.Z. Yin, W.H. Yang, Z. Wang, Y. Zhang, M.C. Zhu, C. Dou, Y. Che, S.J. Sun, C. Hu, B. Teng, J.Q. Zhao, J.Y. Lu, R.Y. Sun, D.G. Zhong, Achieving zero-thermal quenching luminescence in ZnGa_2O_4 : 0.02Eu^{3+} red phosphor. *J. Alloy Compd.* **898**, 162786 (2022)
43. X.L. Wu, R. Shi, J.L. Zhang, D.W. Wen, Z.X. Qiu, X.G. Zhang, W.L. Zhou, L.P. Yu, S.X. Lian, Highly efficient and zero-thermal-quenching blue-emitting Eu^{2+} -activated K-beta-alumina phosphors. *Chem. Eng. J.* **429**, 132225 (2022)
44. S.H. Wang, Y.Q. Xu, T. Chen, W.H. Jiang, J.M. Liu, X. Zhang, W. Jiang, L.J. Wang, A red phosphor $\text{LaSc}_3(\text{BO}_3)_4$: Eu^{3+} with zero-thermal-quenching and high quantum efficiency for LEDs. *Chem. Eng. J.* **404**, 125912 (2021)
45. S.Q. Piao, Y.C. Wang, X.F. Zhou, W.Y. Geng, J.S. Zhang, X.Z. Zhang, D.Y. Wu, Y.Z. Cao, X.P. Li, B.J. Chen, Defect engineering in a Eu^{2+} -doped beta- Al_2O_3 structure blue phosphor and its controllable zero-thermal quenching luminescence. *ACS Sustain. Chem. Eng.* **9**, 7882–7890 (2021)

46. X.G. Zhang, Z.P. Zhu, Z.Y. Guo, F.W. Mo, Z.C. Wu, A zero-thermal-quenching and color-tunable phosphor LuVO_4 : Bi^{3+} , Eu^{3+} for NUV LEDs. *Dyes Pigments* **156**, 67–73 (2018)
47. R. Shi, L.X. Ning, Z.Q. Wang, J.T. Chen, T.K. Sham, Y. Huang, Z.M. Qi, C.J. Li, Q. Tang, H.B. Liang, Zero-thermal quenching of Mn^{2+} red luminescence via efficient energy transfer from Eu^{2+} in BaMgP_2O_7 . *Adv. Opt. Mater.* **7**, 1901187 (2019)
48. J. Crapse, N. Pappireddi, M. Gupta, S.Y. Shvartsman, E. Wieschaus, M. Wuhr, Evaluating the Arrhenius equation for developmental processes. *Mol. Syst. Biol.* **17**, e9895 (2021)
49. L.Z. Liu, R.Y. Liu, T. Xu, Q. Zhang, Y.B. Tan, Q.L. Zhang, J.D. Ding, Y.F. Tang, Enhanced catalytic oxidation of chlorobenzene over MnO_2 grafted in situ by rare earth oxide: surface doping induces lattice oxygen activation. *Inorg. Chem.* **59**, 14407–14414 (2020)
50. N. Zhou, P. Gao, Y. Yang, Y. Zhong, M. Xia, Y. Zhang, Y. Tian, X. Lu, Z. Zhou, Novel orange–red emitting phosphor $\text{Sr}_8\text{ZnY}(\text{PO}_4)_7$: Sm^{3+} with enhanced emission based on Mg^{2+} and Al^{3+} incorporation for plant growth LED lighting. *J. Taiwan Inst. Chem. E* **104**, 360–368 (2019)
51. G. Lakshminarayana, A.N. Meza-Rocha, O. Soriano-Romero, E.F. Huerta, U. Caldino, A. Lira, D.E. Lee, J. Yoon, T. Park, Analysis of fluorescence characteristics of Sm^{3+} -doped B_2O_3 -rich glasses for Orange-light-emitting diodes. *J. Alloy Compd.* **884**, 161076 (2021)
52. S. Verma, D. Kumar, S. Dutta, V. Sharma, H.C. Swart, V. Kumar, A novel near white light emitting phosphor $\text{KSrYSi}_2\text{O}_7$: Dy^{3+} : synthesis, characterization and luminescence properties. *Vacuum* **174**, 109179 (2020)
53. C. Liu, Z. Xia, Z. Lian, J. Zhou, Q. Yan, Structure and luminescence properties of green-emitting $\text{NaBaScSi}_2\text{O}_7$: Eu^{2+} phosphors for near-UV-pumped light emitting diodes. *J. Mater. Chem. C* **1**, 7139–7147 (2013)
54. M. Gao, C. Peng, X. Dong, G. Xue, A. Wang, Y. Pan, A red phosphor of $\text{Ba}_3\text{In}_2\text{F}_{12}$: Mn^{4+} with enhanced moisture stability for warm WLED application. *J. Lumin.* **242**, 118564 (2022)
55. Y. Xu, L. Zhang, S. Yin, X. Wu, H. You, Highly efficient green-emitting phosphors with high color rendering for WLEDs. *J. Alloy Compd.* **911**, 165149 (2022)
56. Q. Liu, Z. Chen, X. Chen, Y. Zhu, W. Chen, S. Liu, P. Chen, T. Yuan, B. Wei, Eu^{3+} and Mn^{4+} co-doped BaLaMgNbO_6 double perovskite phosphors for WLED application. *J. Lumin.* **246**, 118808 (2022)

Publisher's Note Springer Nature remains neutral with regard to jurisdictional claims in published maps and institutional affiliations.

Springer Nature or its licensor (e.g. a society or other partner) holds exclusive rights to this article under a publishing agreement with the author(s) or other rightsholder(s); author self-archiving of the accepted manuscript version of this article is solely governed by the terms of such publishing agreement and applicable law.